ICASSP 2026 - 2026 IEEE International Conference on Acoustics, Speech and Signal Processing (ICASSP) | 979-8-3315-6701-9/26/$31.00 ©2026 IEEE | DOI: 10.1109/ICASSP55912.2026.11465068

SPARSE RECOVERY USING TIGHT FRAMES AND MINIMAX CONCAVE PENALTY

Kartheek Kumar Reddy Nareddy[†‡], *Abhishek Shreekant Bhandiwad*[†],
Abijith Jagannath Kamath[†] and Chandra Sekhar Seelamantula[†]

[†]Department of Electrical Engineering, Indian Institute of Science, Bengaluru, India.
[‡] Institute of Data Science, German Aerospace Center, Jena, Germany.

ABSTRACT

Sparse signal recovery is an important problem in compressed sensing, signal/image processing, computational imaging and machine learning. The design of the sensing matrix is crucial in compressed sensing. While random Gaussian sensing matrices are relatively easier to construct, it is known that matrices constituting a tight frame provide superior reconstruction performance. We formulate the problem of sparse signal recovery using a new data-fidelity term that effectively "tightens" the sensing matrix, and incorporate the minimax concave penalty (MCP) instead of the ℓ_1-norm for promoting sparsity. We carry out the optimization using a proximal gradient method and its Nesterov accelerated counterpart. Simulation results demonstrate that the proposed algorithms result in up to three times faster convergence and superior reconstruction accuracy over benchmark methods.

Index Terms— Sparse recovery, tight frames, back-projection loss, minimax concave penalty, nonconvex optimization

1. INTRODUCTION

Recovering sparse signals from compressed measurements is of significant interest in various signal and image processing problems [1] and several computational imaging applications such as compressed sensing image recovery [2], optical-coherence tomography [3], seismic imaging [4], magnetic resonance imaging [5], single-pixel camera [6], radar imaging [7], etc. In compressed sensing [8], the signal of interest $\boldsymbol{x}^* \in \mathbb{R}^n$ is assumed to have a sparse representation in a suitable basis. The compressed measurements take the form

$$\boldsymbol{y} = \mathbf{A}\boldsymbol{x}^* + \boldsymbol{w}, \tag{1}$$

where $\mathbf{A} \in \mathbb{R}^{m\times n}$, $m \ll n$ denotes the *sensing matrix*, and $\boldsymbol{w} \in \mathbb{R}^m$ denotes the measurement noise. By exploiting sparsity, one can recover $\boldsymbol{x}^*$ from compressed linear measurements $\boldsymbol{y}$ ideally by solving the ℓ_0-minimization problem

$$\underset{\boldsymbol{x}\in\mathbb{R}^n}{\text{minimize}} \ \|\boldsymbol{x}\|_0, \quad \text{subject to } \|\mathbf{A}\boldsymbol{x} - \boldsymbol{y}\|_2 \leq \epsilon, \tag{2}$$

where $\|\cdot\|_0$-pseudonorm is the count of the number of nonzero entries in its argument. Since the optimization problem is combinatorially complex, greedy methods such as matching pursuit and its variants [9–11] or iterative-thresholding-based methods [12] arrive at approximate solutions to (2). However, they are susceptible to noise. A computationally viable alternative is to replace the objective function in (2) by the ℓ_1-norm. If the sensing matrix satisfies the *restricted isometry property (RIP)* [13], then the solutions to both problems are equivalent with a very high probability. The unconstrained version of the ℓ_1-minimization (ℓ_1-regularized least-squares) problem takes the following form:

$$\underset{\boldsymbol{x}\in\mathbb{R}^n}{\text{minimize}} \ \frac{1}{2}\|\mathbf{A}\boldsymbol{x} - \boldsymbol{y}\|_2^2 + \lambda\|\boldsymbol{x}\|_1, \tag{3}$$

where $\lambda > 0$ is a regularization parameter that trades-off between data-fidelity and sparsity. The optimization problem in (3) can be solved using proximal gradient methods such as iterative shrinkage thresholding algorithm (ISTA) [14], its fast variant (FISTA) [15], approximate message passing (AMP) algorithms [16], and deep-unfolding based neural network methods [17–19].

While the ℓ_1-regularized least-squares problem has been widely used for applications in sparse recovery owing to convexity, nonconvex approximations to the ℓ_0-pseudonorm have been shown to provide superior estimates [19–27]. In particular, the amplitude estimation accuracy can be improved using the minimax concave penalty (MCP) [23] as suggested in [26, 28]. It was shown in [23] that the MCP provides nearly unbiased amplitude estimates in comparison to ℓ_1-minimization. As the name suggests, the MCP is obtained as the minimizer of a certain measure of maximum concavity. The MCP itself is nonconvex, but it lends itself to efficient computation of the proximal operator thereby enabling the development of proximal gradient methods. More precisely, the proximal operator of the MCP turns out to be piecewise linear and provides unbiased estimates particularly for large amplitude coefficients.

The design of the sensing matrix is crucial in compressed sensing. Sensing matrices that constitute a Parseval tight frame have been shown to minimize the recovery error [29]. On the other hand, the construction of Gaussian sensing matrices is relatively simple. In this paper, we use a generalized data-fidelity term that effectively *tightens* the sensing matrix, given non-tight Gaussian sensing matrix. We consider the MCP as the sparsity-promoting regularizer for solving the sparse signal recovery problem.

1.1. Contributions of This Paper

We employ the recently proposed tight-frame data-fidelity loss [30] or the backprojection loss [31] coupled with the MCP (Section 3). We solve the sparse recovery problem using an iterative proximal gradient method and its accelerated counterpart. Experimental results showing faster convergence and superior reconstruction accuracy over the benchmark methods are reported in Section 4. Before proceeding further, we recall essential mathematical preliminaries pertaining to tight frames and the minimax concave penalty (Section 2).

This work is funded by the Science and Engineering Research Board (SERB). The code to reproduce the results in this paper is available at https://github.com/AbhishekSB23/TF-MCP.

Authorized licensed use limited to: Deutsches Zentrum fuer Luft- und Raumfahrt. Downloaded on November 03,2026 at 13:40:12 UTC from IEEE Xplore. Restrictions apply.

2. MATHEMATICAL PRELIMINARIES

2.1. Tight Frames and Compressed Sensing

A set of n vectors $\{\boldsymbol{v}_i \in \mathbb{R}^m\}_{i=1}^n$, $n \geq m$, is said to constitute a *frame* [32, 33] for $\mathbb{R}^m$ if there exist constants α and β, $0 < \alpha \leq \beta < \infty$ such that $\forall \boldsymbol{x} \in \mathbb{R}^n$, the following partial-energy equivalence holds:

$$\alpha \|\boldsymbol{x}\|_2^2 \leq \sum_{i=1}^{n} |\langle \boldsymbol{x}, \boldsymbol{v}_i \rangle|^2 \leq \beta \|\boldsymbol{x}\|_2^2 . \tag{4}$$

We have a *tight frame* if $\alpha = \beta$, and a *Parseval tight frame* if $\alpha = \beta = 1$. Stacking the vectors in the form of a matrix $\mathbf{V} = [\boldsymbol{v}_1 \ \boldsymbol{v}_2 \cdots \boldsymbol{v}_n] \in \mathbb{R}^{m \times n}$, the Parseval tight-frame property can be expressed as a matrix property: $\mathbf{V}\mathbf{V}^\mathsf{T} = \mathbf{I}$, where $\mathbf{I}$ denotes the identity matrix. Effectively, $\mathbf{V}$ is the left-inverse of $\mathbf{V}^\mathsf{T}$, and we refer to $\mathbf{V}$ as a *tight-frame matrix*.

Let $\mathbf{A} = [\boldsymbol{a}_1 \ \boldsymbol{a}_2 \cdots \boldsymbol{a}_n] \in \mathbb{R}^{m \times n}$ denote the sensing matrix. Incoherence between the columns of $\mathbf{A}$ and a smaller spread in its singular values result in accurate sparse recovery. More precisely, it has been shown that equiangular tight frames (ETFs) achieve the lowest coherence, *i.e.*, the Welch bound [13], in which case, any pair of columns in $\mathbf{A}$ have the same coherence. A hurdle, however, is that the existence of ETFs for arbitrary choices of m and n is not guaranteed. Moreover, construction of an ETF is a challenging problem [34, 35]. In comparison, Gaussian sensing matrices are relatively easier to construct and satisfy the RIP with a high probability [13]. Therefore, Gaussian sensing matrices are typically preferred to ETFs in compressed sensing applications. Our endeavour is to bridge Gaussian sensing matrices and tight frames.

2.2. Minimax Concave Penalty

The measure of maximum concavity of a differentiable function $h : [0, +\infty) \to \mathbb{R}$ is defined as

$$\kappa(h) = \sup_{0 < x_1 < x_2} \frac{h'(x_1) - h'(x_2)}{x_2 - x_1}, \tag{5}$$

where h' denotes the derivative of h. It can be shown that $\kappa(h)$ is bounded below by 0 when h is concave. A concave function h satisfies

$$\begin{aligned} h(x_2) &\leq h(x_1) + h'(x_1)(x_2 - x_1), \quad \text{and} \\ h(x_1) &\leq h(x_2) + h'(x_2)(x_1 - x_2), \end{aligned}$$

for all $x_1, x_2 \in \mathbb{R}$. Summing the two inequalities, we get $(h'(x_1) - h'(x_2))(x_2 - x_1) \geq 0$, for all $x_1, x_2 \in \mathbb{R}$. Therefore, $x_2 > x_1 > 0 \implies h'(x_2) - h'(x_1) \leq 0 \implies \kappa(h) \geq 0$. The minimax concave penalty is obtained by minimizing $\kappa(h)$ subject to certain boundary conditions, as recalled next.

Theorem 1 (Minimax concave penalty [28])**.** *A differentiable, concave function $h : [0, +\infty) \to \mathbb{R}$ that satisfies the boundary conditions $h(0) = h(0^+) = 0, h'(x) = 0, \forall x \geq \gamma\lambda, h'(0^+) = \lambda, \gamma > 1, \lambda > 0$, and minimizes the measure of maximum concavity $\kappa(h)$ is given by*

$$h(x) = \begin{cases} \lambda x - \dfrac{x^2}{2\gamma}, & x < \lambda\gamma, \\ \dfrac{\lambda^2\gamma}{2}, & x \geq \lambda\gamma. \end{cases} \tag{6}$$

The MCP $g : \mathbb{R} \to \mathbb{R}$ is constructed by symmetrizing h as $g(x) = h(|x|)$. The proximal operator of g is given by [28]

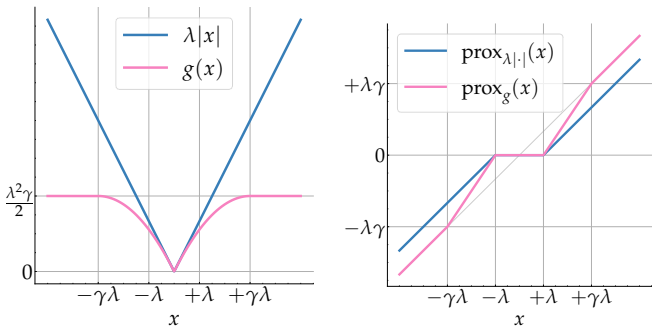


Fig. 1: Comparison of (a) sparsity promoting penalties and (b) the corresponding proximal operators.

$$\begin{aligned} \operatorname{prox}_g(x) &= \arg\min_{y \in \mathbb{R}} \ \frac{1}{2}(x - y)^2 + g(y), \\ &= \min\left\{ |x|, \max\left\{ \frac{\gamma}{\gamma - 1}(|x| - \lambda), 0 \right\} \right\} \operatorname{sgn}(x), \end{aligned} \tag{7}$$

where sgn denotes the signum function. Fig. 1 compares MCP and the ℓ_1-norm and their proximal operators.

3. SPARSE RECOVERY USING TIGHT FRAMES AND THE MINIMAX CONCAVE PENALTY

Consider the canonical sparse recovery problem with a $\mathbf{B}$-norm data-fidelity term:

$$\underset{\boldsymbol{x} \in \mathbb{R}^n}{\text{minimize}} \ \frac{1}{2} \|\boldsymbol{y} - \mathbf{A}\boldsymbol{x}\|_{\mathbf{B}}^2 + g(\boldsymbol{x}), \tag{8}$$

where $g(\boldsymbol{x})$ is the MCP and operates element-wise on its arguments. The sensing matrix $\mathbf{A} \in \mathbb{R}^{m \times n}$ is assumed to have full row-rank and unit ℓ_2-norm columns. For the choice of $\mathbf{B} = \left(\mathbf{A}\mathbf{A}^\mathsf{T}\right)^{-\frac{1}{2}}$, the data-fidelity term equals

$$\frac{1}{2} \|\boldsymbol{y} - \mathbf{A}\boldsymbol{x}\|_{\mathbf{B}}^2 = \frac{1}{2} \left\| \mathbf{A}^\dagger (\boldsymbol{y} - \mathbf{A}\boldsymbol{x}) \right\|_2^2,$$

where $\mathbf{A}^\dagger = \mathbf{A}^\mathsf{T}\left(\mathbf{A}\mathbf{A}^\mathsf{T}\right)^{-1}$ denotes the right pseudoinverse of $\mathbf{A}$. Recall that $\mathbf{A}$ is assumed to have full row-rank, which ensures the existence of $\mathbf{B}$. It is verifiable that the effective sensing matrix $\mathbf{B}\mathbf{A}$ constitutes a Parseval tight-frame. In this paper, we employ the formulation in (8) with $\mathbf{B} = \left(\mathbf{A}\mathbf{A}^\mathsf{T}\right)^{-\frac{1}{2}}$ for sparse recovery and use proximal gradient methods to solve the optimization problem. The benchmark methods used for comparison are ISTA [14], FISTA [15], TF variants — TF-ISTA, TF-FISTA, RTF-ISTA, and RTF-FISTA from [30]. RTF-ISTA and RTF-FISTA are rescaled-gradient versions of TF-ISTA and TF-FISTA, respectively, derived by normalizing the columns of the effective sensing matrix. For more details, the reader is referred to [30]. We also adapt these algorithms to include MCP instead of ℓ_1 for accurate sparse recovery. The resulting algorithms are called TF-MCP, its Nesterov accelerated variant TF-FMCP, and their rescaled gradient versions RTF-MCP and RTF-FMCP, and their updates are listed below.

Authorized licensed use limited to: Deutsches Zentrum fuer Luft- und Raumfahrt. Downloaded on November 03,2026 at 13:40:12 UTC from IEEE Xplore. Restrictions apply.

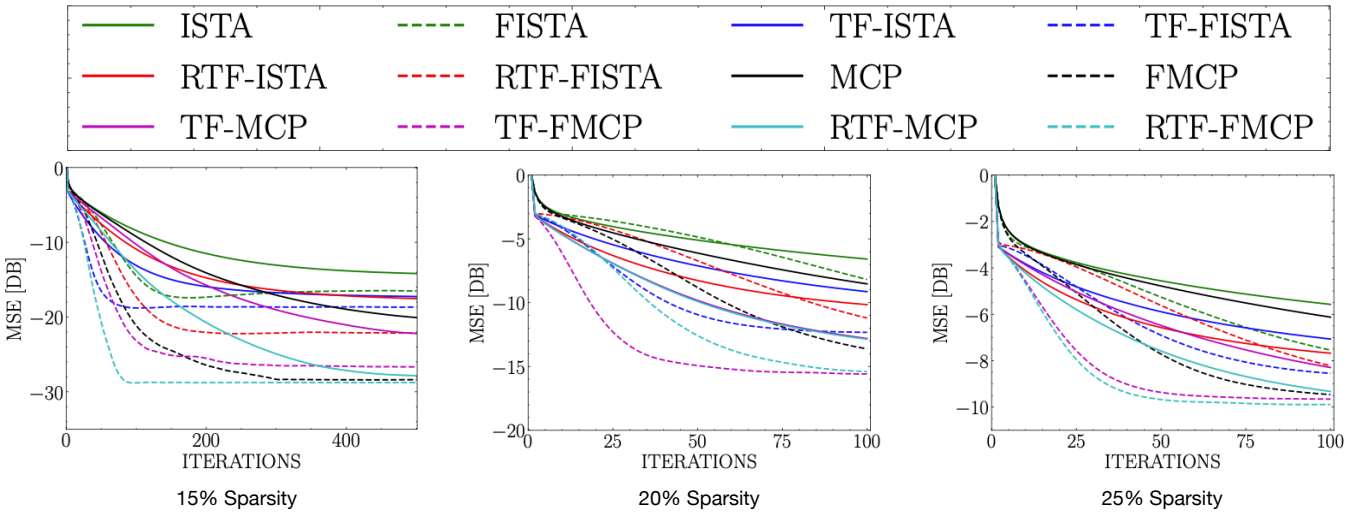


Fig. 2: Performance comparison of the techniques under consideration: MSE (dB) vs. iterations for measurements obtained with 50% compression ratio at 50 dB SNR for varying sparsity levels. The plots show that the TF-FMCP and RTF-FMCP techniques converge faster than the benchmark techniques. At 15% sparsity, RTF-FMCP converges in about 100 iterations, while FMCP converges in about 300 iterations to provide similar performance.

- The MCP update is given by

$$\boldsymbol{x}_{k+1} = \text{prox}_{\eta g}\left(\boldsymbol{x}_k - \eta \mathbf{A}^{\mathsf{T}}(\mathbf{A}\boldsymbol{x}_k - \boldsymbol{y})\right), \tag{9}$$

  where $0 < \eta < 1$ is the step-size parameter. The $\text{prox}_{\eta g}$ operator is given in (7).
- The FMCP (fast MCP) updates are given by

$$\begin{aligned} \boldsymbol{x}_{k+1} &= \text{prox}_{\eta g}\left(\boldsymbol{z}_k - \eta \mathbf{A}^{\mathsf{T}}(\mathbf{A}\boldsymbol{z}_k - \boldsymbol{y})\right), \\ t_{k+1} &= \frac{1+\sqrt{1+4t_k^2}}{2}, \\ \boldsymbol{z}_{k+1} &= \boldsymbol{x}_{k+1} + \left(\frac{t_k - 1}{t_{k+1}}\right)(\boldsymbol{x}_{k+1} - \boldsymbol{x}_k), \end{aligned} \tag{10}$$

  where $t_0 = 1$, $\boldsymbol{z}_0 = \boldsymbol{x}_0 = \mathbf{A}^{\dagger}\boldsymbol{y}$.
- The TF-MCP update is given by

$$\boldsymbol{x}_{k+1} = \text{prox}_{\eta g}\left(\boldsymbol{x}_k - \eta \mathbf{A}^{\dagger}(\mathbf{A}\boldsymbol{x}_k - \boldsymbol{y})\right). \tag{11}$$

- The rescaled tight-frame MCP (RTF-MCP) update is given by

$$\boldsymbol{x}_{k+1} = \text{prox}_{\eta g}\left(\boldsymbol{x}_k - \eta \mathbf{C}^{-1}\mathbf{A}^{\dagger}(\mathbf{A}\boldsymbol{x}_k - \boldsymbol{y})\right), \tag{12}$$

  where $\mathbf{C} = \left(\mathbf{A}^{\dagger}\mathbf{A}\right) \odot \mathbf{I}$, $\odot$ denotes the Hadamard product.
- The TF-FMCP (fast TF-MCP) updates are given by

$$\begin{aligned} \boldsymbol{x}_{k+1} &= \text{prox}_{\eta g}\left(\boldsymbol{z}_k - \eta \mathbf{A}^{\dagger}(\mathbf{A}\boldsymbol{z}_k - \boldsymbol{y})\right), \\ t_{k+1} &= \frac{1+\sqrt{1+4t_k^2}}{2}, \\ \boldsymbol{z}_{k+1} &= \boldsymbol{x}_{k+1} + \left(\frac{t_k - 1}{t_{k+1}}\right)(\boldsymbol{x}_{k+1} - \boldsymbol{x}_k), \end{aligned} \tag{13}$$

- The RTF-FMCP (fast RTF-MCP) updates are given by

$$\begin{aligned} \boldsymbol{x}_{k+1} &= \text{prox}_{\eta g}\left(\boldsymbol{z}_k - \eta \mathbf{C}^{-1}\mathbf{A}^{\dagger}(\mathbf{A}\boldsymbol{z}_k - \boldsymbol{y})\right), \\ t_{k+1} &= \frac{1+\sqrt{1+4t_k^2}}{2}, \\ \boldsymbol{z}_{k+1} &= \boldsymbol{x}_{k+1} + \left(\frac{t_k - 1}{t_{k+1}}\right)(\boldsymbol{x}_{k+1} - \boldsymbol{x}_k). \end{aligned} \tag{14}$$

4. EXPERIMENTAL VALIDATION

We consider experiments on simulated synthesis-sparse signals. The support for the ground-truth sparse signal $\boldsymbol{x}^* \in \mathbb{R}^{1000}$ is selected using a uniform distribution, while the amplitudes are drawn from a normal distribution. The sparsity factor ρ is defined to be $\|\boldsymbol{x}^*\|_0/n$. The elements in the sensing matrix $\mathbf{A} \in \mathbb{R}^{m\times n}$ are *i.i.d.* following the standard Gaussian distribution $\mathcal{N}(0,1)$. The columns of the sensing matrix $\mathbf{A} \in \mathbb{R}^{m\times n}$ are rescaled to have unit ℓ_2-norm. The measurement vector $\boldsymbol{y} \in \mathbb{R}^m$ is constructed as $\boldsymbol{y} = \mathbf{A}\boldsymbol{x}^* + \boldsymbol{w}$, where $\boldsymbol{w}$ is a Gaussian noise vector with entries having zero mean and variance σ^2. One hundred realizations $\{\boldsymbol{x}_i^*\}_{i=1}^{100}$ are generated and the corresponding reconstructions $\{\hat{\boldsymbol{x}}_i^*\}_{i=1}^{100}$ are obtained. Sparse signal recovery is performed using the techniques proposed in Section 3 and the benchmark techniques. The performance is quantified in terms of the mean-squared error (MSE) and reconstruction signal-to-noise-ratio (RSNR):

$$\begin{aligned} \text{MSE} &= 20\cdot\log_{10}\left(\frac{\sum_{i=1}^{100}\|\hat{\boldsymbol{x}}_i - \boldsymbol{x}_i^*\|_2}{\sum_{i=1}^{100}\|\boldsymbol{x}_i^*\|_2}\right)\text{dB}, \\ \text{RSNR} &= \frac{1}{100}\sum_{i=1}^{100} 20\cdot\log_{10}\left(\frac{\|\boldsymbol{x}_i^*\|_2}{\|\hat{\boldsymbol{x}}_i - \boldsymbol{x}_i^*\|_2}\right)\text{dB}. \end{aligned} \tag{15}$$

Fig. 2 compares the iterate convergence of the methods under consideration for various sparsity levels. Notably, RTF-FMCP

Authorized licensed use limited to: Deutsches Zentrum fuer Luft- und Raumfahrt. Downloaded on November 03,2026 at 13:40:12 UTC from IEEE Xplore. Restrictions apply.

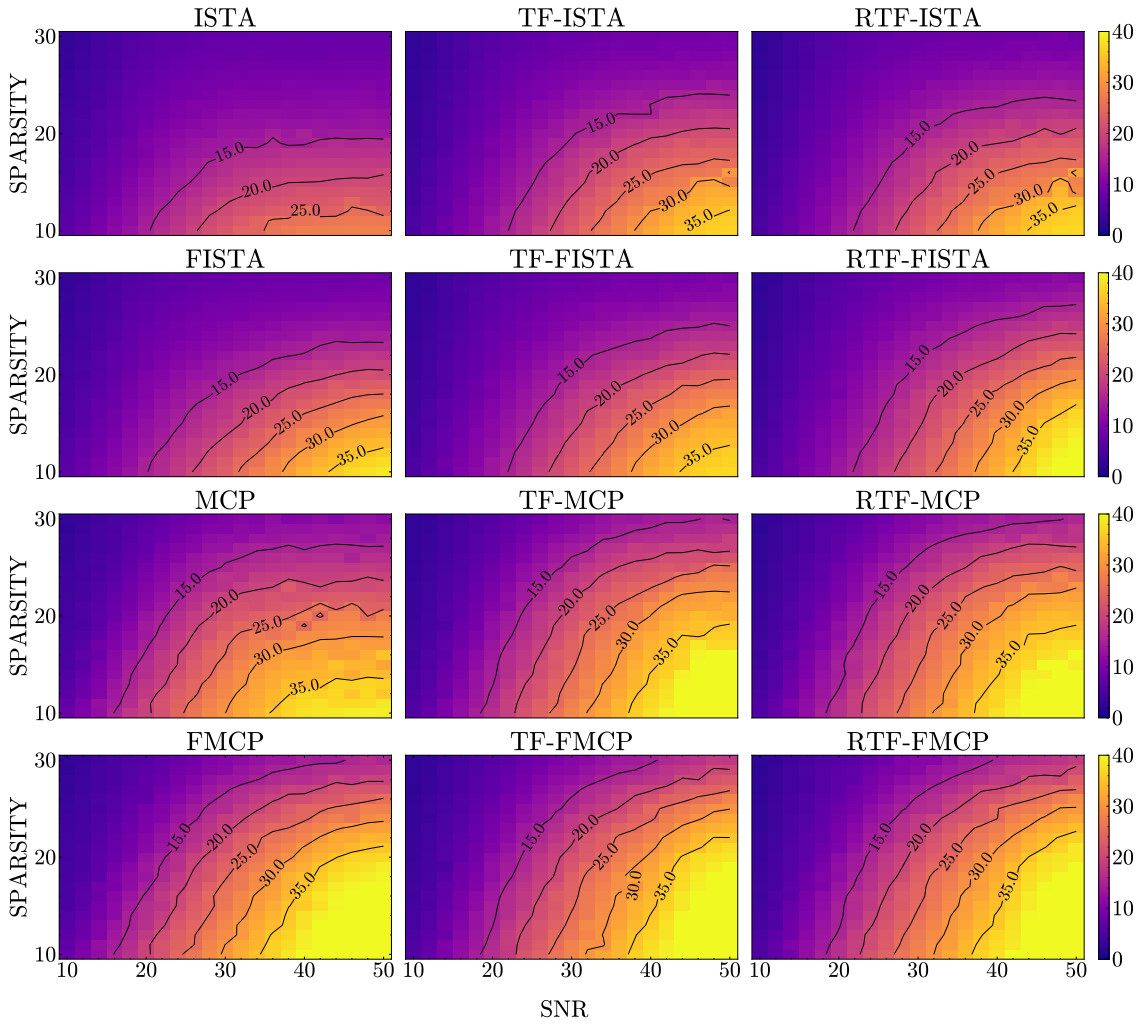


Fig. 3: RSNR comparison of various sparse recovery techniques for 50% compression ratio. The figure reveals that TF-MCP and RTF-MCP demonstrate superior performance compared to MCP. As the sparsity factor increases (corresponding to a higher number of non-zeros in the reconstructed signal), TF-FMCP outperforms FMCP. However, at higher noise levels (lower SNR values), FMCP exhibits superior performance compared to TF-FMCP.

demonstrates the fastest convergence at 15% sparsity, reaching convergence within 100 iterations, compared to 300 iterations of FMCP. At 20% sparsity, TF-FMCP is the fastest with convergence achieved in 50 iterations, followed by RTF-FMCP at 100 iterations and FMCP at 150 iterations. In the 25% sparsity scenario, both TF-FMCP and RTF-FMCP outperform the other methods in terms of speed of convergence. In general, TF/RTF-MCP versions are better than the benchmark methods. Fig. 3 compares the RSNR, as a function of SNR and sparsity, for various sparse signal recovery methods (for 50% compression ratio). The contours delineate RSNR levels. The bright pixels indicate high RSNR and dark pixels indicate low RSNR. Notably, TF-MCP and RTF-MCP demonstrate substantial performance improvements over MCP. FMCP and RTF-FMCP exhibit similar performance, with TF variants slightly outperforming MCP at higher sparsity levels. Conversely, FMCP shows a slight advantage over TF variants at low SNRs. A similar observation was made in the context of analysis-sparse ℓ_1 penalty in [30].

5. CONCLUSIONS

In this paper, we integrated non-convex regularization functions, specifically the MCP, for sparse recovery with tight-frame data-fidelity to obtain tight-frame minimax concave penalty (TF-MCP) algorithm. Further, we accelerated the reconstruction by incorporating Nesterov's momentum, resulting in the TF-FMCP algorithm. Rescaled variants, namely RTF-MCP and RTF-FMCP, were derived by normalizing the columns of the effective sensing matrix. The experiments show that sparse recovery with a tight-frame sensing matrix provides superior performance compared to non-tight-frame matrices. Between MCP and ℓ_1 regularizers, the former outperforms the latter. A combination of the tight-frame data-fidelity and its variants improve the performance over standard least-squares. Specifically, rescaling the gradients helps accelerate convergence and provides the best performance. The techniques TF-FMCP and RTF-FMCP converge the fastest and provide the best reconstruction performance overall. In summary, sparse recovery performance improves with one or more of the following — tight-frame data-fidelity, minimax concave penalty, and rescaled gradients.

Authorized licensed use limited to: Deutsches Zentrum fuer Luft- und Raumfahrt. Downloaded on November 03,2026 at 13:40:12 UTC from IEEE Xplore. Restrictions apply.

6. REFERENCES

[1] M. Elad, *Sparse and Redundant Representations: From Theory to Applications in Signal and Image Processing*, Springer, 1st edition, 2010.

[2] W. Dong, G. Shi, X. Li, Y. Ma, and F. Huang, "Compressive sensing via nonlocal low-rank regularization," *IEEE Trans. Image Process.*, vol. 23, no. 8, pp. 3618–3632, 2014.

[3] S. Mukherjee and C. S. Seelamantula, "Fienup algorithm with sparsity constraints: Application to frequency-domain optical-coherence tomography," *IEEE Trans. on Sig. Proces.*, vol. 62, no. 18, pp. 4659–4672, 2014.

[4] S. Mache et al., "Introducing nonuniform sparse proximal averaging network for seismic reflectivity inversion," *IEEE Trans. on Comput. Imaging*, pp. 1–14, 2023.

[5] W. Lu and N. Vaswani, "Modified compressive sensing for real-time dynamic MR imaging," in *Proc. IEEE Intl. Conf. on Image Proces. (ICIP)*, 2009, pp. 3045–3048.

[6] M. F. Duarte, M. A. Davenport, D. Takhar, J. N. Laska, T. Sun, K. F. Kelly, and R. G. Baraniuk, "Single-pixel imaging via compressive sampling," *IEEE Signal Process. Mag.*, vol. 25, no. 2, pp. 83–91, 2008.

[7] M. A. Herman and T. Strohmer, "High-resolution radar via compressed sensing," *IEEE Trans. on Sig. Proces.*, vol. 57, no. 6, pp. 2275–2284, 2009.

[8] D. L. Donoho, "Compressed sensing," *IEEE Trans. Inf. Theory*, vol. 52, no. 4, pp. 1289–1306, 2006.

[9] S. G. Mallat and Z. Zhang, "Matching pursuits with time-frequency dictionaries," *IEEE Trans. Signal Process.*, vol. 41, no. 12, pp. 3397–3415, 1993.

[10] D. Needell and J. A. Tropp, "CoSaMP: Iterative signal recovery from incomplete and inaccurate samples," *Appl. Comput. Harmon. Anal.*, vol. 26, no. 3, pp. 301–321, 2009.

[11] R. G. Baraniuk, V. Cevher, M. F. Duarte, and C. Hegde, "Model-based compressive sensing," *IEEE Trans. Inf. Theory*, vol. 56, no. 4, pp. 1982–2001, 2010.

[12] T. Blumensath and M. E. Davies, "Iterative hard thresholding for compressed sensing," *Appl. Comput. Harmon. Anal.*, vol. 27, no. 3, pp. 265–274, 2009.

[13] S. Foucart and H. Rauhut, *A Mathematical Introduction to Compressive Sensing*, Applied and Numerical Harmonic Analysis. Springer New York, 2013.

[14] I. Daubechies, M. Defrise, and C. De Mol, "An iterative thresholding algorithm for linear inverse problems with a sparsity constraint," *Comm. Pure Appl. Math.*, vol. 57, no. 11, pp. 1413–1457, 2004.

[15] A. Beck and M. Teboulle, "A fast iterative shrinkage-thresholding algorithm with application to wavelet-based image deblurring," in *Proc. IEEE Int. Conf. Acoust., Speech, Signal Process. (ICASSP)*, 2009, pp. 693–696.

[16] D. L. Donoho, A. Maleki, and A. Montanari, "Message-passing algorithms for compressed sensing," *Proc. Natl. Acad. Sci.*, vol. 106, no. 45, pp. 18914–18919, 2009.

[17] K. Gregor and Y. LeCun, "Learning fast approximations of sparse coding," in *Proc. Int. Conf. Mach. Learn. (ICML)*, 2010, p. 399–406.

[18] J. Liu and X. Chen, "ALISTA: Analytic weights are as good as learned weights in LISTA," in *Proc. Int. Conf. Learn. Represent. (ICLR)*, 2019.

[19] P. K. Pokala, A. G. Mahurkar, and C. S. Seelamantula, "Firm-Net: A sparsity amplified deep network for solving linear inverse problems," in *IEEE Int. Conf. Acoust. Speech Signal Process. (ICASSP)*. IEEE, 2019, pp. 2982–2986.

[20] K. Bredies and D. A. Lorenz, "Iterated hard shrinkage for minimization problems with sparsity constraints," *SIAM Journ. on Scient. Comput.*, vol. 30, no. 2, pp. 657–683, 2008.

[21] S. Foucart and M. J. Lai, "Sparsest solutions of underdetermined linear systems via ℓ_q-minimization for $0 < q \leq 1$," *Appl. Comput. Harmon. Anal.*, vol. 26, no. 3, 2009.

[22] J. Fan and R. Li, "Variable selection via nonconcave penalized likelihood and its oracle properties," *J. Amer. Statist. Assoc.*, vol. 96, no. 456, pp. 1348–1360, 02 2001.

[23] C. H. Zhang, "Nearly unbiased variable selection under minimax concave penalty," *The Ann. Stat.*, vol. 38, no. 2, pp. 894–942, 2010.

[24] E. Chouzenoux et al., "A Majorize-Minimize subspace approach for $\ell_2 - \ell_0$ image regularization," *SIAM J. Imaging Sci.*, vol. 6, no. 1, pp. 563–591, 2013.

[25] P. Yin et al., "Minimization of ℓ_{1-2} for compressed sensing," *SIAM J. Sci. Comput.*, vol. 37, no. 1, pp. A536–A563, 2015.

[26] Ivan Selesnick, "Sparse regularization via convex analysis," *IEEE Transactions on Signal Processing*, vol. 65, no. 17, pp. 4481–4494, 2017.

[27] H. Mohimani, M. Babaie-Zadeh, and C. Jutten, "A fast approach for overcomplete sparse decomposition based on smoothed ℓ^0 norm," *IEEE Trans. Signal Process.*, vol. 57, no. 1, pp. 289–301, 2009.

[28] P. K. Pokala, R. V. Hemadri, and C. S. Seelamantula, "Iteratively reweighted minimax-concave penalty minimization for accurate low-rank plus sparse matrix decomposition," *IEEE Trans. Pattern Anal. Mach. Intell.*, vol. 44, no. 12, pp. 8992–9010, 2021.

[29] W. Chen, M. R. D. Rodrigues, and I. J. Wassell, "Projection design for statistical compressive sensing: A tight frame based approach," *IEEE Trans. Signal Process.*, vol. 61, no. 8, pp. 2016–2029, 2013.

[30] K. K. R. Nareddy, A. J. Kamath, and C. S. Seelamantula, "Tight-frame-like analysis-sparse recovery using nontight sensing matrices," *SIAM Journal on Imaging Sciences*, vol. 17, no. 3, pp. 1587–1618, 2024.

[31] T. Tirer and R. Giryes, "Back-projection based fidelity term for ill-posed linear inverse problems," *IEEE Trans. on Image Process.*, vol. 29, pp. 6164–6179, 2020.

[32] J. Kovačević and A. Chebira, "Life beyond bases: The advent of frames (Part I)," *IEEE Signal Process. Mag.*, vol. 24, no. 4, pp. 86–104, 2007.

[33] J. Kovačević and A. Chebira, "Life beyond bases: The advent of frames (Part II)," *IEEE Signal Process. Mag.*, vol. 24, no. 5, pp. 115–125, 2007.

[34] P.W.H Lemmens and J.J Seidel, "Equiangular lines," *Journal of Algebra*, vol. 24, no. 3, pp. 494–512, 1973.

[35] J. H. Conway, R. H. Hardin, and N. J.A. Sloane, "Packing lines, planes, etc.: Packings in Grassmannian spaces.," *Experimental Mathematics*, vol. 5, no. 2, pp. 139–159, 1996.

Authorized licensed use limited to: Deutsches Zentrum fuer Luft- und Raumfahrt. Downloaded on November 03,2026 at 13:40:12 UTC from IEEE Xplore. Restrictions apply.